**Climate
of the Past**
Open Access

Discussions

^{10}Be in late deglacial climate simulated by ECHAM5-HAM – Part 2: Isolating the solar signal from ^{10}Be deposition

U. Heikkilä[1], X. Shi[2], S. J. Phipps[3], and A. M. Smith[1]

[1]Australian Nuclear Science and Technology Organisation (ANSTO), Lucas Heights, NSW, Australia
[2]Centre for Atmospheric Chemistry, University of Wollongong, NSW, Australia
[3]ARC Centre of Excellence for Climate System Science and Climate Change Research Centre, University of New South Wales, Australia

Correspondence to: U. Heikkilä (ulla.heikkilae@eawag.ch)

CPD

9, 5627–5657, 2013

^{10}**Be in deglaciation – Part 2: Isolating solar signal**

U. Heikkilä et al.

Title Page

Abstract | Introduction

Conclusions | References

Tables | Figures

|◄ | ►|

◄ | ►

Back | Close

Full Screen / Esc

Printer-friendly Version

Interactive Discussion

Abstract

This study investigates the effect of deglacial climate on the deposition of the solar proxy ^{10}Be globally, and at two specific locations, the GRIP site at Summit, Central Greenland, and the Law Dome site in coastal Antarctica. The deglacial climate is represented by three 30 yr time slice simulations of 10 000 BP (years before present = 1950 CE), 11 000 BP and 12 000 BP, compared with a preindustrial control simulation. The model used is the ECHAM5-HAM atmospheric aerosol–climate model, driven with sea surface temperatures and sea ice cover simulated using the CSIRO Mk3L coupled climate system model. The focus is on isolating the ^{10}Be production signal, driven by solar variability, from the weather or climate driven noise in the ^{10}Be deposition flux during different stages of climate. The production signal varies on lower frequencies, dominated by the 11 yr solar cycle within the 30 yr time scale of these experiments. The climatic noise is of higher frequencies. We first apply empirical orthogonal functions (EOF) analysis to global ^{10}Be deposition on the annual scale and find that the first principal component, consisting of the spatial pattern of mean ^{10}Be deposition and the temporally varying solar signal, explains 64 % of the variability. The following principal components are closely related to those of precipitation. Then, we apply ensemble empirical decomposition (EEMD) analysis on the time series of ^{10}Be deposition at GRIP and at Law Dome, which is an effective method for adaptively decomposing the time series into different frequency components. The low frequency components and the long term trend represent production and have reduced noise compared to the entire frequency spectrum of the deposition. The high frequency components represent climate driven noise related to the seasonal cycle of e.g. precipitation and are closely connected to high frequencies of precipitation. These results firstly show that the ^{10}Be atmospheric production signal is preserved in the deposition flux to surface even during climates very different from today's both in global data and at two specific locations. Secondly, noise can be effectively reduced from ^{10}Be deposition data by simply applying the EOF analysis in the case of a reasonably large number of avail-

able data sets, or by decomposing the individual data sets to filter out high-frequency fluctuations.

1 Introduction

Reconstruction of solar activity has so far only been possible for the Holocene (e.g.
Steinhilber et al., 2012; Vonmoos et al., 2006). Evidence of the existence of solar cycles during the last ice age was found by Wagner et al. (2001) in the [10]Be record from the GRIP ice core between 25 and 50 kyr BP, but a continuous record extending from the Holocene into the preceding ice age is still missing. During the last deglaciation the solar proxies [10]Be and ^{14}C exhibited significant, climate driven, differences, which complicates the extraction of the solar signal (e.g. Muscheler et al., 2004). In order to study the climate impact on [10]Be during the last deglaciation we perform time slice model simulations during three stages: 10 000 ("10k"), 11 000 ("11k") and 12 000 ("12k") BP (years before 1950 CE), compared with a control ("ctrl") simulation during the preindustrial climate. The mean climate change as well as the mean difference in [10]Be deposition and atmospheric distribution has been analysed in an accompanying manuscript (Heikkilä et al., 2013). The main findings are that the lower greenhouse gas concentrations in the deglaciation simulations influence the climate, leading to a tropospheric cooling and drying and changes in sea ice cover which affect atmospheric circulation patterns. However, these changes were found to cause [10]Be deposition to fluctuate by no more than 50 % locally, although changes in air concentrations and dry deposition were significantly larger than that. The results indicate that [10]Be deposition is mostly driven by mass balance. The amount of [10]Be produced in the atmosphere is deposited to the surface within a few years and therefore, averaged over a few years, the deposition equals production.

While the accompanying study concentrates on spatial differences as influenced by the mean state of the climate, this study focuses on temporal changes and investigates how the 11 yr solar signal in [10]Be production is preserved in the global and local

deposition flux. The aim is to assess how much the production signal is distorted by climatic noise in these simulations. We first focus on global deposition and quantify the different components of the variability, production and climate-related "noise", with the aid of empirical orthogonal function (EOF) analysis. Then, because observations do
5 not cover the entire globe but are limited to a few locations we analyse time series of the modelled [10]Be deposition at two locations: the GRIP drilling site in Greenland and the Law Dome site in Antarctica.

The traditional approach to detect solar cycles in [10]Be records has been to create a frequency, for example a Fourier, spectrum which reveals the known solar cy-
10 cles, e.g. ~ 11 (Schwabe), ~ 22 (Hale), ~ 88 (Gleissberg), ~ 205 (de Vries) and ~ 2300 (Hallstatt) yr (e.g. McCracken et al., 2012). Bandpass filtering has been used to distinguish between solar and geomagnetic modulation of [10]Be production by assuming that fluctuations with frequencies below a given threshold, typically 1000 yr, are due to geomagnetic variations whereas high-frequency fluctuations are due to solar variability
15 (Beer et al., 1994, 2002; Wagner et al., 2001). The drawback of using the Fourier spectrum to detect frequency peaks is that the length of each solar cycle is assumed to be constant in time. However, the length of the cycles has been found to be non constant and is currently under much investigation (e.g. Richards et al., 2009). Already during the 30 yr period investigated within this study each of the three ca. 11 yr cycles varies
20 by ±1 yr in length. Bandpass filtering, on the other hand, requires a priori knowledge of the frequencies of the cycles to set the frequency limits. To overcome these potentially limiting assumptions we propose the ensemble empirical mode decomposition (EEMD) method (Huang and Wu, 2008; Huang et al., 1998; Wu and Huang, 2009) in this study. EEMD decomposes the [10]Be signal into a set of frequency components, termed intrin-
25 sic mode functions (IMFs). As this decomposition is based on the local characteristics of the data, it offers a potentially viable method for nonlinear and nonstationary data analysis, especially for time-frequency representation. The IMFs, therefore, have no set frequency but are allowed to vary with time. Moreover, the IMFs represent the entire frequency spectrum of the data and not only a preset frequency range. The IMFs

resulting from EEMD analysis can then be combined to be associated with solar or geomagnetic forcing on [10]Be data.

EEMD has widely been used in time series analysis, such as surface temperature (Franzke, 2012), tree ring data (Shi et al., 2012) and changes in onset of seasons (Qian et al., 2009), but, to our knowledge, never in combination with [10]Be. This study focuses on the level of distortion of the solar signal in [10]Be deposition due to deglacial climate changes. Model data is useful to test the suitability of EEMD for this study because the solar signal used is known. While the length of the model data (30 yr) restricts the type of solar cycles to be studied to only the 11 yr one, EEMD can be applied to real-world data including a larger number of cycles in the future. The only [10]Be observations available from the last deglaciation are from the GISP2 ice core (Finkel and Nishiizumi, 1997) but their temporal resolution of 20–50 yr does not compare with the monthly resolution of this study. Holocene observations covering several solar cycles typically have an annual or longer temporal resolution. Sub-annually resolved observations are limited in length and typically include up to one 11 yr cycle only. This prohibits a direct comparison with the current model data.

2   Methods

Here we only give general information on the model simulations and refer to the accompanying paper (Heikkilä et al., 2013) for details. The model used is the atmospheric aerosol–climate model ECHAM5-HAM which incorporates radionuclide production, transport and deposition processes. To produce deglacial climate the model is driven with sea surface temperatures and sea ice cover obtained from simulations using the CSIRO Mk3L climate system model version 1.2 (Phipps et al., 2011, 2012). Each of the ECHAM5-HAM model simulations (ctrl, 10k, 11k and 12k) represents a 30 yr time slice of an equilibriated state of climate during these periods. The [10]Be production during the last deglaciation is based on a ^{14}C reconstruction with a modern 11 yr cycle added on top (Heikkilä et al., 2013). It is thus theoretical and does not

Full Screen / Esc

Printer-friendly Version

Interactive Discussion

allow the results to be quantitively compared with observations. Analysis of the mean changes in climate and in atmospheric [10]Be transport and deposition are provided by Heikkilä et al. (2013).

We first apply the empirical orthogonal functions (EOF) analysis, also known as prin-
5   cipal component analysis, to global [10]Be data in this study. This method was introduced by Lorenz (1956) and has since been widely used in climate data analysis to detect patterns such as the North Atlantic oscillation or the Southern Annular Mode in sea level pressure data, among various others. It creates a linear combination of a number of orthogonal spatial patterns (referred to as EOFs in this manuscript), multiplied by a time
10 series component (referred to as PCs). Because the global [10]Be deposition fields comprise a temporally varying component, the production signal, but also vary spatially due to differences in the precipitation patterns and location of the stratosphere–troposphere exchange, this method seems suitable for removing noise and reducing the dimensionality of [10]Be data.
15 The words "signal" and "noise" will be used throughout the manuscript to refer to the solar variability driven atmospheric production (signal) and climate driven fluctuations (noise) in [10]Be deposition data. Both components typically have very distinctive time scales. The production varies on multi-year time scales, such as the 11 yr cycle. Shorter term fluctuations in the solar activity parameter cause high-frequency fluctuations in the
20 production rate but these are efficiently filtered out by the atmospheric transport from the stratosphere to the troposphere. Climate related changes, the largest of which is the seasonal cycle of e.g. precipitation rate, act on sub-annual time scales. Long-term trends in climatic variables are also possible but were not found during the relatively short simulations of 30 yr each. In order to decompose the [10]Be deposition into various
25 frequencies we apply the EEMD method to [10]Be deposition and the precipitation rate at GRIP and Law Dome, for each of the four simulations. We aim to analyse the raw data without applying any averaging or filtering. However, seasonal fluctuations of [10]Be data are of much larger amplitude than solar modulation and have to be removed. We apply

[10]Be in deglaciation – Part 2: Isolating solar signal

U. Heikkilä et al.

Title Page

Abstract | Introduction

Conclusions | References

Tables | Figures

|◄ | ►|

◄ | ►

Back | Close

Full Screen / Esc

Printer-friendly Version

Interactive Discussion

a simple 25 month running mean to smooth out the seasonal cycle but only minimally reduce the length of the data set, consistent with Heikkilä et al. (2013).

The EEMD method decomposes time series into intrinsic mode functions (IMF), each of which represents a specific frequency range, and a long-term trend. The first IMF has the highest frequency and so on. The sum of these IMFs and the long-term trend reproduces the original time series. The length of the time series determines the number of IMFs. Our time series consist of monthly 30 yr data, smoothed with a 25 month running mean, adding up to 336 data points. This creates seven IMFs and a long-term trend. Each of the model simulations is analysed separately, because the data has to be continuous for EEMD, and then combined.

The EEMD analysis can be briefly summarised as follows:

1. Add white noise with a predefined noise amplitude to the data to be analysed.

2. Run EMD to decompose the data with added white noise into IMFs.

3. Repeat the above steps several times to create the ensembles.

4. The final results are obtained as ensemble means of corresponding IMFs of the decomposition.

3 Results

3.1 EOF analysis of global ^{10}Be deposition

In the following we analyse the temporal variability of the simulated global ^{10}Be deposition flux. In order to detect the solar cycle in the ^{10}Be flux it is necessary to remove the seasonal cycle which has been found to dominate temporal variability on short time scales (Heikkilä and Smith, 2013). Therefore, we analyse 25 month running mean values. The mean distribution of ^{10}Be deposition over each 30 yr simulation is shown in Fig. 1. We apply EOF analysis for the three-dimensional deposition field with all four

simulations combined to produce the common EOFs for each simulation. The first EOF obtained is shown in Fig. 2 together with the three first principal components. The first EOF (top panel) explains 64 % of the variability and is very similar to the mean ^{10}Be deposition pattern (Fig. 1). The first principal component, shown in blue, correlates strongly ($r = 0.92$) with the 11 yr solar cycle (green). The delay of ca. 1 yr between the production (solar) and the deposition signal reflects the atmospheric residence time of ^{10}Be (e.g. Beer et al., 1990). The following EOFs are fairly patternless and exhibit significant variability only in the tropics (not shown). The tropics are generally not best suited for recording ^{10}Be as a solar proxy due to the low production variability and the uplifting of air due to the Brewer–Dobson circulation. Therefore the tropical tropospheric air is less enriched by stratospheric ^{10}Be, which exhibits the largest production variability, and the ^{10}Be signal in tropical tropospheric air includes more noise. The corresponding two following PCs (in blue) explain 23 % and 5 % of the variability and the rest of them less than 5 % each. It seems that the variability of the internal climate modes, described by these PCs, was not amplified in the deglaciation simulations. The standard deviations ("std" shown in the figure) are slightly reduced relative to ctrl in the deglaciation simulations, especially at 12k. However the mean value of the second PC at 12k is higher.

The first PC thus represents the production signal and the following PCs the climate-related noise. In order to investigate if the noise components are related to climatic variability we perform EOF analysis for the 25 month running mean precipitation fields. The PCs are very similar to the noise components of the ^{10}Be deposition, suggesting that the climatic noise is closely related to precipitation variability. The first three precipitation PCs are shown in Fig. 3 (green) together with the second to fourth PCs of ^{10}Be deposition (blue). The PCs of precipitation explain 59 % (1st), 13 % (2nd) and 11 % (3rd) of the variability. The correlation coefficients (0.98 to 0.81) suggest that these are closely related to the second to fourth PCs of ^{10}Be deposition.

Given these results the ^{10}Be deposition can be decomposed into a spatial deposition pattern which is similar to the climatological mean deposition pattern multiplied by the

temporally varying production signal plus noise, which can thus be discarded. Even during deglacial climate the production signal seems large enough to make full use of the method. These results suggest that this method can therefore be applied to observations as well. However, observational records might not be easily combined due to their different temporal resolution and coverage, variable quality and very limited spatial coverage. In reality, insufficient observations are available to fully distinguish signal from noise.

3.2 EEMD analysis of ^{10}Be deposition at GRIP and at Law Dome

Typically these complications restrict the number of time series which can be analysed collectively. Hence, principal component analysis might not be able to reveal the solar signal during periods when observations disagree. Therefore we apply an alternative method, the EEMD, to analyse time series separately at two particular locations: the GRIP site in central Greenland (72°35′ N, 37°38′ W, 3216 m a.s.l.) and the Law Dome site in coastal Antarctica (66°46.18′ S, 112°48.69′ E, 1370 m a.s.l.). Both are characterised by relatively high snow accumulation and therefore a number of high resolution time series exist (e.g. Muscheler et al., 2005; Pedro et al., 2011; Yiou et al., 1997).

We first present the modelled time series of ^{10}Be deposition at both sites (Fig. 4) for all four simulations. Both monthly mean and 25 month running mean values are shown. The monthly fluctuations are considerable in all simulations at both stations but smoothing the seasonal cycle out (25 month running mean) reveals the solar cycle. The three ca. 11 yr solar cycles are seen in all simulations at both stations, however some distortion is visible, especially at 12k. The mean value of ^{10}Be deposition only varies by ca. 5 % between these stations. While the global mean deposition has to be constant in all simulations, local changes of up to 50 % could have been expected based on the analysis of the mean climate (Heikkilä et al., 2013). The precipitation rate (Fig. 5) does vary more at GRIP, exhibiting reduced monthly variability and a lower mean at 12k than in other simulations. At Law Dome, the mean precipitation rate and the standard deviation are gradually reduced at 12k relative to ctrl. It seems that the

^{10}Be in deglaciation – Part 2: Isolating solar signal

U. Heikkilä et al.

Title Page

Abstract | Introduction

Conclusions | References

Tables | Figures

◄ | ►

◄ | ►

Back | Close

Full Screen / Esc

Printer-friendly Version

Interactive Discussion

reduced precipitation rate at 12k does not therefore affect the mean [10]Be deposition at 12k; however, it might contribute to the high amplitude of variability in the reconstructed production signal at 12k.

Figure 6 shows the data as input for the EEMD analysis, with the 25 month running mean [10]Be production, deposition and precipitation rate. The production rate shown is the global mean. The data is normalised through division by the mean, showing that the amplitude of the deposition variability is comparable with the global mean production rate variability. The [10]Be deposition follows the three solar cycles shown by the production rate in all simulations at both stations. The [10]Be deposition is delayed in exhibiting the second production minimum in the 11k simulation at GRIP, which could be due to the large simultaneous peak in the precipitation rate. Given the length of the time series, the EEMD analysis results in seven intrinsic mode functions (IMFs). These are shown in Figs. 7 and 8. In addition, a long term trend is obtained (IMF8). The sum of these IMFs and the trend reproduces the original data. The first three IMFs are interpreted as climate-related noise as their frequency is less than annual. The following five IMFs (4–8) are considered to represent the solar signal, or [10]Be production rate. Which IMFs are attributed to signal and noise is ambiguous and depends on the time resolution of the data. In our case, sub-annual variations can only be of climatic origin and can be discarded as noise. It might be advantageous to vary the number of the IMFs used to reconstruct the production as closely to the original solar signal as possible in each simulation, but in case of observations the actual signal is not known. We therefore aim to create a standard methodology based on physically justified thresholds which can be applied to any data without prior knowledge of the reconstructed signal.

The high-frequency components IMF1–2 do not vary significantly between the simulations at GRIP. Only the IMF3 fluctuates more strongly at 12k (standard deviation 10–60 % higher). The IMF5 is closest to the [10]Be production signal, exhibiting the three ca. 11 yr solar cycles. However, the first cycle of IMF5 is shorter than the solar one, for which the IMF6 contributes by creating the broader shoulder seen during the first

third of each 30 yr period. This suggests a stronger climatic impact on ^{10}Be deposition during this period, seen as anomalously low precipitation rate at ctrl, 10k and 11k (Fig. 6). The IMF7 has a similar form but is flat in 10k, however its amplitude is negligible compared with other IMFs. At Law Dome the noise components (IMF1–3) are fairly similar in amplitude in all simulations. IMF4 has a lower frequency in ctrl than in the other simulations, and it contributes more to the two last solar cycles than IMF5, which nearly misses them. Such a shift towards higher-frequencies suggests stronger climate impact during the last solar cycle. This is consistent with the higher amplitude of the high-frequency IMFs of precipitation (not shown) which seems to distort the solar signal in ^{10}Be deposition. Also the percentage of total variability explained by noise is larger at 7 % than in other simulations (see the following subsection). IMF7 is very flat in ctrl and 10k but has a distinctive pattern in 11k and 12k but again the amplitude is too small to be detected in the total signal.

The reconstructed production signal from the ^{10}Be deposition (IMF4–8) is illustrated in Fig. 9 for both stations, together with the original production rate. Removing the high-frequency noise flattens the signal and increases the agreement with production (compare with Fig. 6). The data sets have been normalised for comparison. The amplitude of the reconstructed production agrees reasonably well with the actual production, but is slightly underestimated at GRIP and overestimated at Law Dome in 11k. The second production maximum is underestimated in 12k at both stations. This was already seen in the original data (Fig. 6) and cannot be improved by removing the high-frequency noise. Figure 10 shows the reconstructed high-frequency part of the spectrum (IMF1–3) of both the ^{10}Be deposition and precipitation. They have been standardised to allow for comparison. Generally the variability seems similar in all simulations and both stations. Both noise components seem correlated, especially in the case of 10k, 11k and 12k at GRIP and 10k and 11k at Law Dome. In ctrl the precipitation noise fluctuates more strongly than ^{10}Be deposition noise at both stations. The variability explained by the signal and the noise components is shown in the figures as well. The signal components dominate the variability explaining 93–97 % of total variability at both stations.

Title Page

Abstract | Introduction

Conclusions | References

Tables | Figures

◀◀ | ▶▶

◀ | ▶

Back | Close

Full Screen / Esc

Printer-friendly Version

Interactive Discussion

The variability contribution of all IMFs is shown in Fig. 11. The first three IMFs are negligible at both stations and all simulations. At GRIP, the IMF5, which is very closely related to the solar signal (see Fig. 7), explains nearly 70 % of total variability in ctrl. However, in the deglacial simulations this contribution is reduced and IMF4 and the long term trend get more weight. At Law Dome there is no single dominant IMF, but IMFs 4–5 (and the long-term trend in case of deglacial simulations) are most dominant. Apparently IMF7, albeit exhibiting distinct differences between the simulations, is not of importance for the total variability in any of the simulations. Combining results of both stations suggests that in the 12k simulation there is a significant long-term trend, which is absent in ctrl. Furthermore, the Law Dome station seems more strongly affected by the climatic noise than GRIP in these simulations.

In order to distinguish the effect of noise reduction from production signal we analyse correlations between variables. Figure 12 shows scatter plots of normalised ^{10}Be deposition and precipitation, and ^{10}Be production and deposition at GRIP. ^{10}Be deposition and production (signal) are shown without (IMF1–8; blue) and with (IMF4–8; red) filtering of high-frequency noise, ^{10}Be deposition and precipitation (noise) only without filtering because of the different scales of the variables (IMF1–3 have zero mean due to the subtraction of the long-term mean and thus different scale). However, correlation coefficients are shown for both the unfiltered (IMF1–8; first) and the filtered (IMF1–3; second) data. Comparison of the unfiltered and filtered correlations indicates that filtering the high-frequency noise improves the agreement between ^{10}Be deposition and production signals, however, the difference is not large. This is due to the strong 11 yr cycle which causes the data to be autocorrelated, dominating the correlation. Therefore the correlation coefficients should be interpreted as indicative only. However, we do not attempt to remove the autocorrelation because the 11 yr cycle is the very part of the ^{10}Be production signal which we are trying to detect. In case of the noise components (^{10}Be deposition and precipitation) there seems to be no connection between them in the unfiltered data, indicated by the low correlation coefficients. Filtering out the production signal, i.e. the 11 yr cycle in case of ^{10}Be, the correlation increases significantly. At

Law Dome the results are similar to GRIP. The correlation of the filtered signal with the production signal is improved from the unfiltered data, albeit only slightly. The noise components of ^{10}Be deposition and precipitation correlate fairly strongly when unfiltered, but the correlation is reduced when the data is filtered. This is due to a similar long-term trend, which, when filtered out, reduces the correlation. Also the fact that white noise is added into the data by the EEMD might reduce the correlation between filtered data sets. Looking at Fig. 6 the precipitation rate at Law Dome seems to exhibit cycles similar in length to the 11 yr cycle, especially in ctrl and 11k. This, however, is coincidental as the model employs a standard radiation scheme with a constant value for solar irradiation. In an atmospheric-only model the climate is constrained mostly by the sea-surface temperatures and sea ice and the solar irradiation plays a minor role.

The physical meaning of these findings is that the temporal variability of ^{10}Be deposition into ice is mostly dominated by the production signal on an annual scale. The correlation between ^{10}Be deposition and production is high, but deteriorates because of fluctuations caused by short-term changes in precipitation rate. If this short-term "climatic" noise is filtered out, the ^{10}Be production signal, reconstructed from the ^{10}Be deposition flux, agrees better with the actual production signal. However, this method only corrects for high-frequency noise, but cannot distinguish longer-term climatic noise from the production signal. This is shown by the fact that the excessively low or high amplitudes of the solar cycles, or the delays in the response to production minima or maxima in ^{10}Be deposition, cannot be corrected for. Still, the EEMD-filtered signal explains more than >95 % of total variability, a result which cannot be achieved by simple bandpass filtering.

4 Summary and conclusions

This study analyses four time slice (30 yr each) simulations of the solar proxy ^{10}Be at different stages of climate: 10 000 BP ("10k"), 11 000 BP ("11k") and 12 000 BP ("12k") during the last deglaciation, compared with a control simulation during the preindustrial

Full Screen / Esc

Printer-friendly Version

Interactive Discussion

period ("ctrl"). We investigate to what extent the different climatic conditions distort the solar signal in the ^{10}Be deposition flux to the surface and how the distortion can be corrected for by analysing the frequency spectrum of the ^{10}Be deposition. The climatic distortion, called noise, is assumed to be represented by the highest frequencies

5 whereas the solar signal is known to vary on a longer time scale. In order to remove the seasonal cycle from the data we first smooth it using 25 month running means.

First, the global field of ^{10}Be deposition is analysed to study the temporal and spatial variability by means of EOF (empirical orthogonal function) analysis, also known as PC (principal component) analysis. We find that the first spatial pattern closely resembles

10 the global deposition field, and the first temporal pattern correlates with the solar signal with $r = 0.92$. 64 % of the total variability of ^{10}Be deposition can be attributed to solar, or production, variability, and 36 % to noise. Analysing the noise components we find close connections between the second and higher temporal patterns and all temporal patterns of precipitation, suggesting that precipitation variability drives the noise part

15 of the ^{10}Be deposition variability after the production signal has been removed. This method allows for noise reduction, as the noise components can be removed. It can be applied to observational data as well, if sufficient spatial coverage is provided and the temporal coverage matches.

As in reality the number of ^{10}Be observations is limited, EOF analysis can pro-

20 duce unreliable results during periods when observations disagree. We propose the use of the ensemble empirical decomposition (EEMD) method, which analyses one-dimensional data. EEMD decomposes the data into intrinsic frequency components without requiring any prior knowledge of these frequencies. Furthermore, it has the advantage of allowing the amplitude and the length of the cycles in the data to vary over

25 time. We decompose the modelled ^{10}Be deposition and precipitation at two particular locations from which a number of ice core records exist: the GRIP site at the summit of Greenland and the Law Dome site in coastal Antarctica. The results are composed of seven intrinsic mode functions with decreasing frequencies and a long-term trend. The high-frequency components are interpreted as climate-driven noise and the low-

frequency ones as the solar signal. The results for GRIP and Law Dome are fairly similar, and removing the high-frequency noise improves the agreement between the [10]Be deposition flux and the production signal. [10]Be deposition at Law Dome includes slightly more climatic noise in these simulations. The amplitude of the reconstructed production signal from the deposition is very similar to the original production. Comparison of the noise components of [10]Be deposition with those of precipitation suggests they are interconnected, in agreement with the results of the global EOF analysis.

These findings support the assumption that, regardless of the state of climate, the variability of [10]Be deposition is dominated by the production variability on annual and longer time scales, simply due to mass conservation. Locally significant fluctuations from the global mean could have been expected but were not found, although the precipitation rate was reduced in the deglacial climate. The EEMD method proved useful in analysing single data series. It was successful in noise reduction and resulted in a deposition signal closer to production, explaining $> 95\%$ of total variability in each simulation, than can be obtained by a simple lowpass filtering or smoothing. However, it was only able to remove high-frequency noise and could not correct for all spurious forms at lower frequencies. EEMD thus seems well suited for noise reduction in single [10]Be time series. We propose it for analysing multi-annually resolved [10]Be records including several solar cycles of various frequencies. Seasonal noise with its amplitude of several factors larger than production variability complicates the analysis of high-resolved records. The strength of EEMD will be the decomposition of the entire frequency spectrum allowing for a distinction of solar cycles of various lengths, as well as the slowly varying strength of the geomagnetic field.

References

Beer, J., Blinov, A., Bonani, G., Finkel, R. C., Hofmann, H. J., Lehmann, B., Oeschger, H., Sigg, A., Schwander, J., Staffelbach, T., Stauffer, B., Suter, M., and Wölfli, W.: Use of ^{10}Be in polar ice to trace the 11-year cycle of solar activity, Nature, 347, 164–166 , 1990. 5634

Beer, J., Baumgartner, S., Dittrich-Hannen, B., Hauenstein, J., Kubik, P., Lukasczyk, C., Mende, W., Stellmacher, R., and Suter, M.: Solar variability traced by cosmogenic isotopes, in: The Sun as a Variable Star: Solar and Stellar Irradiance Variations, edited by: Pap, J. M., Fröhlich, C., Hudson, H. S., and Solanki, S. K., Cambridge University Press, 291–300, 1994. 5630

Beer, J., Muscheler, R., Wagner, G., Laj, C., Kissel, C., Kubik, P. W., and Synal, H.-A.: Cosmogenic nuclides during isotope stages 2 and 3, Quaternary Sci. Rev., 21, 1129–1139, 2002. 5630

Finkel, R. C. and Nishiizumi, K.: Beryllium 10 concentrations in the Greenland Ice Sheet Project 2 ice core from 3–40 ka, J. Geophys. Res., 102, 26699–26706, 1997. 5631

Franzke, C.: Nonlinear trends, long-range dependence and climate noise properties of surface temperature, J. Climate, 25, 4172–4183, doi:10.1175/JCLI-D-11-00293.1, 2012. 5631

Heikkilä, U. and Smith, A. M.: Production rate and climate influences on the variability of ^{10}Be deposition simulated by ECHAM5-HAM: globally, in Greenland and in Antarctica, J. Geophys. Res., 118, 1–15, doi:10.1002/jgrd.50217, 2013. 5633

Heikkilä, U., Phipps, S. J., and Smith, A. M.: ^{10}Be in last deglacial climate simulated by ECHAM5-HAM – Part 1: Climatological influences on ^{10}Be deposition, Clim. Past Discuss., 9, 3681–3709, doi:10.5194/cpd-9-3681-2013, 2013. 5629, 5631, 5632, 5633, 5635

Huang, N. E. and Wu, Z.: A review on Hilbert–Huang transform: method and its applications to geophysical studies, Rev. Geophys. 46, RG2006, doi:10.1029/2007RG000228, 2008. 5630

Huang, N. E., Shen, Z., Long, S. R., Wu, M. C., Shih, H. H., Zheng, Q., Yen, N.-C., Tung, C. C., and Liu, H. H.: The empirical mode decomposition and the Hilbert spectrum for nonlinear and non-stationary time series analysis, P. R. Soc. Lond. A Math., 454, 903–995, 1998. 5630

Lorenz, E. N.: Empirical orthogonal functions and statistical weather prediction, Science Report 1, Statistical forecasting project, Department of meteorology, MIT, NTIS AD 110268, 49 pp., 1956. 5632

McCracken, K., Beer, J., Steinhilber, F., and Abreu, J.: The Heliosphere in time, Space Sci. Rev., 176, 59–71, doi:10.1007/s11214-011-9851-3, 2012. 5630

Muscheler, R., Beer, J., Wagner, G., Laj, C., Kissel, C., Raisbeck, G. M., Yiou, F., and Kubik, P. W.: Changes in the carbon cycle during the last deglaciation as indicated by the comparison of [10]Be and ^{14}C records, EPSL, 6973, 1–16, doi:10.1016/S0012-821X(03)00722-2, 2004. 5629

Muscheler, R., Beer, J., Kubik, P. W., and Synal, H.-A.: Geomagnetic field intensity during the last 60 000 years based on [10]Be & [36]Cl from the Summit ice cores and ^{14}C, Quarternary Sci. Rev., 24, 1849–1860, doi:10.1016/j.quascirev.2005.1001.1012, 2005. 5635

Pedro, J. B., Smith, A. M., Simon, K. J., van Ommen, T. D., and Curran, M. A. J.: High-resolution records of the beryllium-10 solar activity proxy in ice from Law Dome, East Antarctica: measurement, reproducibility and principal trends, Clim. Past, 7, 707–721, doi:10.5194/cp-7-707-2011, 2011. 5635

Phipps, S. J., Rotstayn, L. D., Gordon, H. B., Roberts, J. L., Hirst, A. C., and Budd, W. F.: The CSIRO Mk3L climate system model version 1.0 – Part 1: Description and evaluation, Geosci. Model Dev., 4, 483–509, doi:10.5194/gmd-4-483-2011, 2011. 5631

Phipps, S. J., Rotstayn, L. D., Gordon, H. B., Roberts, J. L., Hirst, A. C., and Budd, W. F.: The CSIRO Mk3L climate system model version 1.0 – Part 2: Response to external forcings, Geosci. Model Dev., 5, 649–682, doi:10.5194/gmd-5-649-2012, 2012. 5631

Qian, C., Fu, C., Wu, Z., and Yan, Z.: On the secular change of spring onset at Stockholm, Geophys. Res. Lett., 36, L12706, doi:10.1029/2009GL038617, 2009. 5631

Richards, M. T., Rogers, M. L., and Richards, D. S. P.: Long-term variability in the length of the solar cycle, Astr. Soc. P., 121, 797–809, doi:10.1086/604667, 2009. 5630

Shi, F., Yang, B., von Gunten, L., Qin, C., and Wang, Z.: Ensemble empirical mode decomposition for tree-ring climate reconstructions, Theor. Appl. Climatol., 109, 233–243, doi:10.1007/s00704-011-0576-8, 2012. 5631

Steinhilber, F., Abreu, J. A., Beer, J., Brunner, I., Christl, M., Fischer, H., Heikkilä, U., Kubik, P. W., Mann, M., McCracken, K. G., Miller, H., Miyahara, H., Oerter, H., and Wilhelms, F.: 9400 years of cosmic radiation and solar activity from ice cores and tree rings, P. Natl. Acad. Sci. USA, 109, 16, 5967–5971, doi:10.1073/pnas.1118965109, 2012. 5629

Vonmoos, M., Beer, J., and Muscheler, R.: Large variations in Holocene solar activity: constraints from [10]Be in the Greenland Ice Core Project ice core, J. Geophys. Res., 111, A01015, doi:10.1029/2005JA011500, 2006. 5629

Title Page

Abstract | Introduction

Conclusions | References

Tables | Figures

|◄ | ►|

◄ | ►

Back | Close

Full Screen / Esc

Printer-friendly Version

Interactive Discussion

Wagner, G., Beer, J., Masarik, J., Muscheler, R., Kubik, P., Mende, W., Laj, C., Raisbeck, G. M., and Yiou, F.: Presence of the solar de Vries cycle (∼205 years) during the last ice age, Geophys. Res. Lett., 28, 303–306, 2001. 5629, 5630

Wu, Z. and Huang, N. E.: Ensemble empirical mode decomposition: a noise-assisted data analysis method, Adv. Adapt. Data Anal., 1, 1–41, 2009. 5630

Yiou, F., Raisbeck, G. M., Baumgartner, S., Beer, J., Hammer, C., Johnsen, S., Jouzel, J., Kubik, P. W., Lestringuez, J., Stiévenard, M., Suter, M., and Yiou, P.: Beryllium 10 in the Greenland Ice Core Project ice at Summit, Greenland, J. Geophys. Res., 102, 26783–26794, 1997. 5635
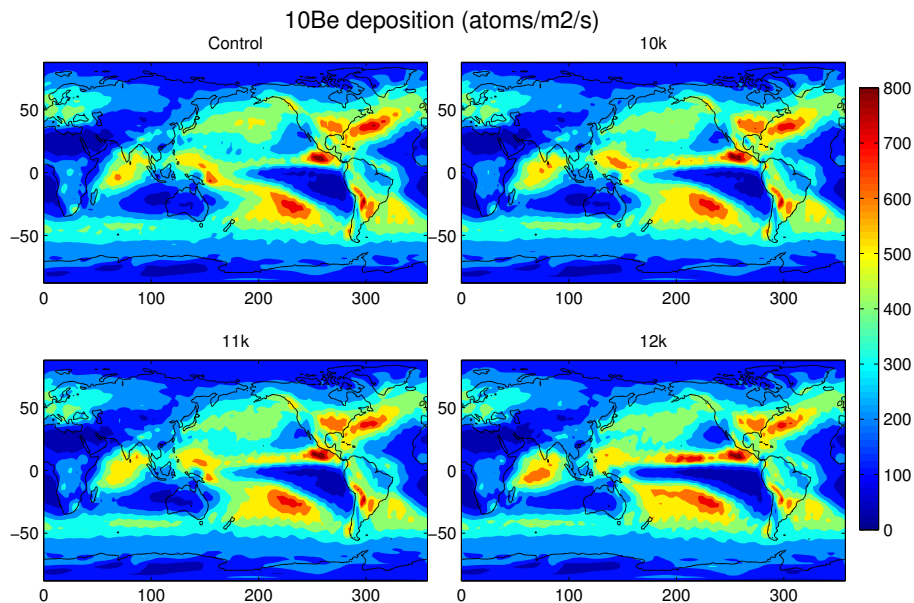
Fig. 1. Mean ^{10}Be deposition (atoms m^{-2} s^{-1}) in the simulations.
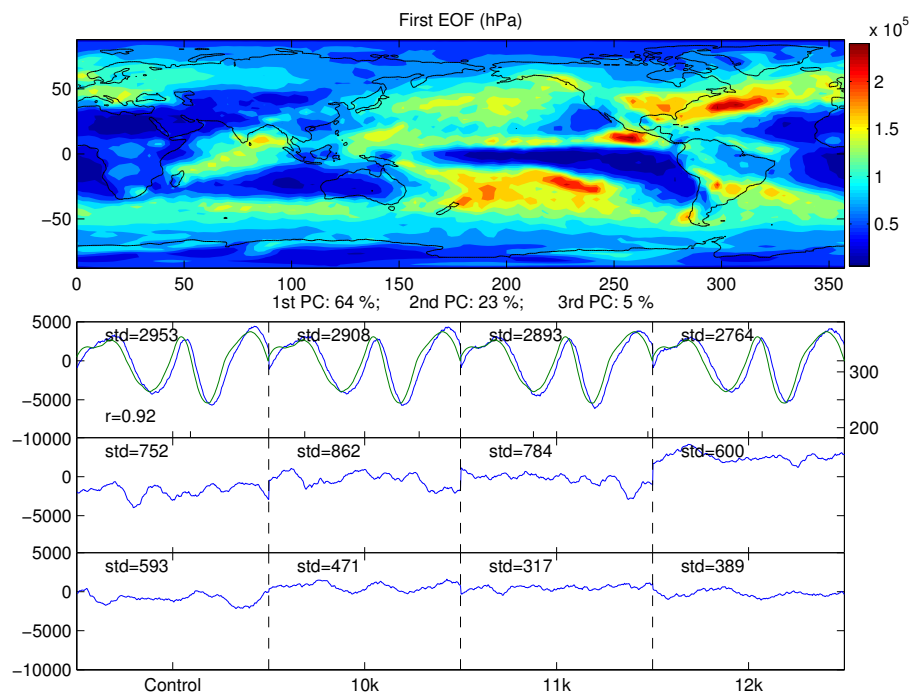
Fig. 2. First empirical orthogonal function (EOF) of the 25 month running mean ^{10}Be deposition. Below the three first principal components (PCs) are shown together with the percentage of deposition variability explained by them for the four simulations (ctrl, 10k, 11k and 12k). The "std" shows the standard deviation of each PC. In addition to the first PC the top panel shows the global ^{10}Be production rate in green and the correlation coefficient with the first PC. Units are normalised.
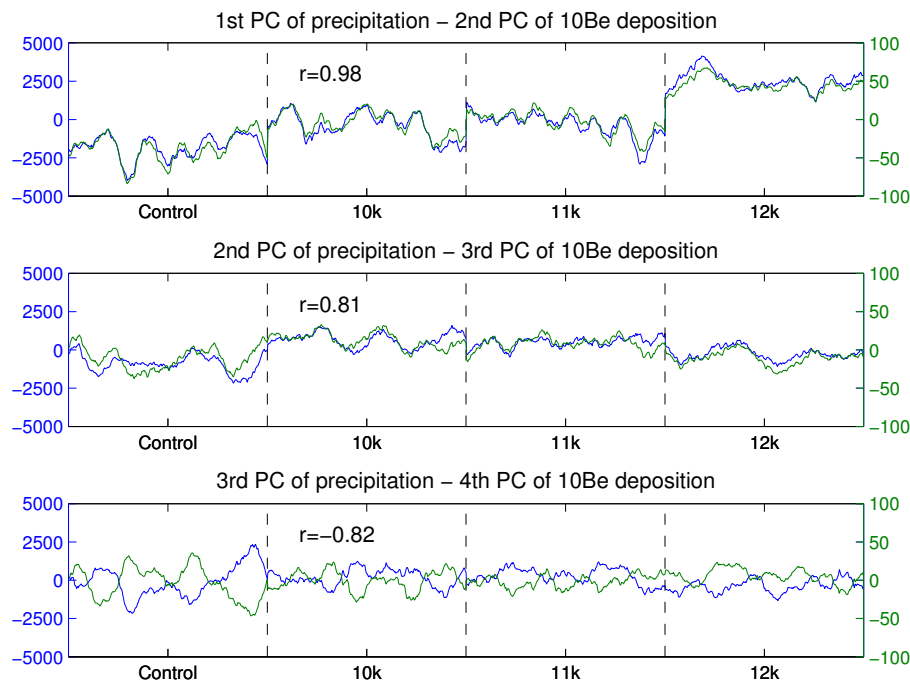
Fig. 3. The second, the third and the fourth principal component (PC) of ^{10}Be deposition (blue) shown with the first three PCs of precipitation (green). The correlation coefficients ("r") are also shown. Units are normalised.

Title Page

Abstract | Introduction

Conclusions | References

Tables | Figures

|◄ | ►|

◄ | ►

Back | Close
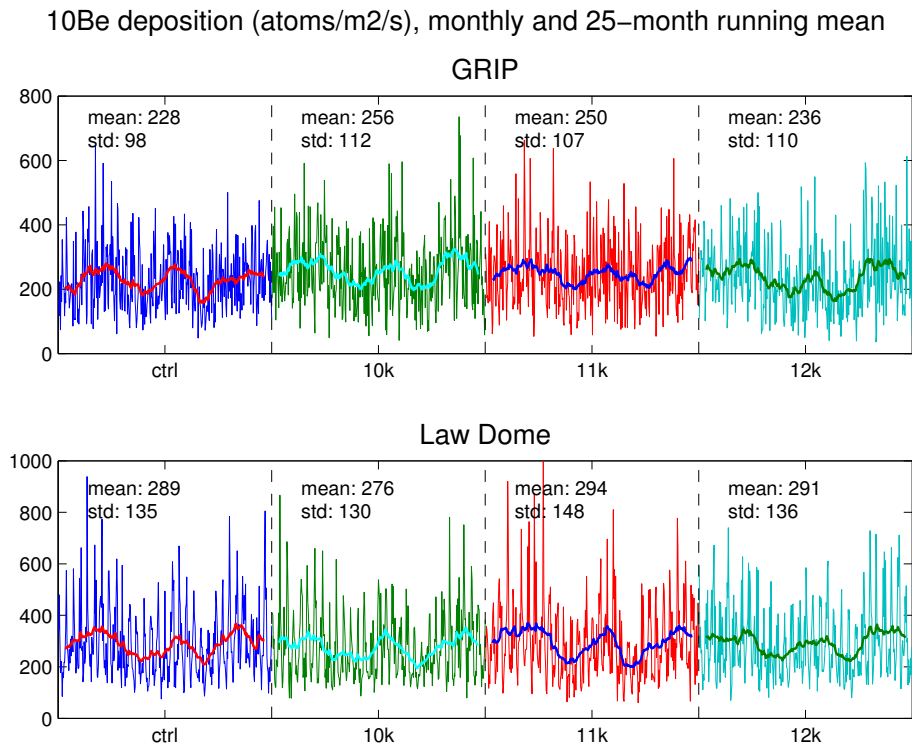
Full Screen / Esc

Fig. 4. ^{10}Be deposition flux (atoms m^{-2} s^{-1}) shown at the GRIP and Law Dome stations, monthly means and 25 month running means.

Precipitation (mm/day), monthly and 25–month running mean

GRIP

mean: 0.63 std: 0.39 | mean: 0.66 std: 0.39 | mean: 0.63 std: 0.35 | mean: 0.49 std: 0.29

Law Dome

mean: 2.93 std: 1.44 | mean: 2.74 std: 1.23 | mean: 2.8 std: 1.24 | mean: 2.5 std: 1.08
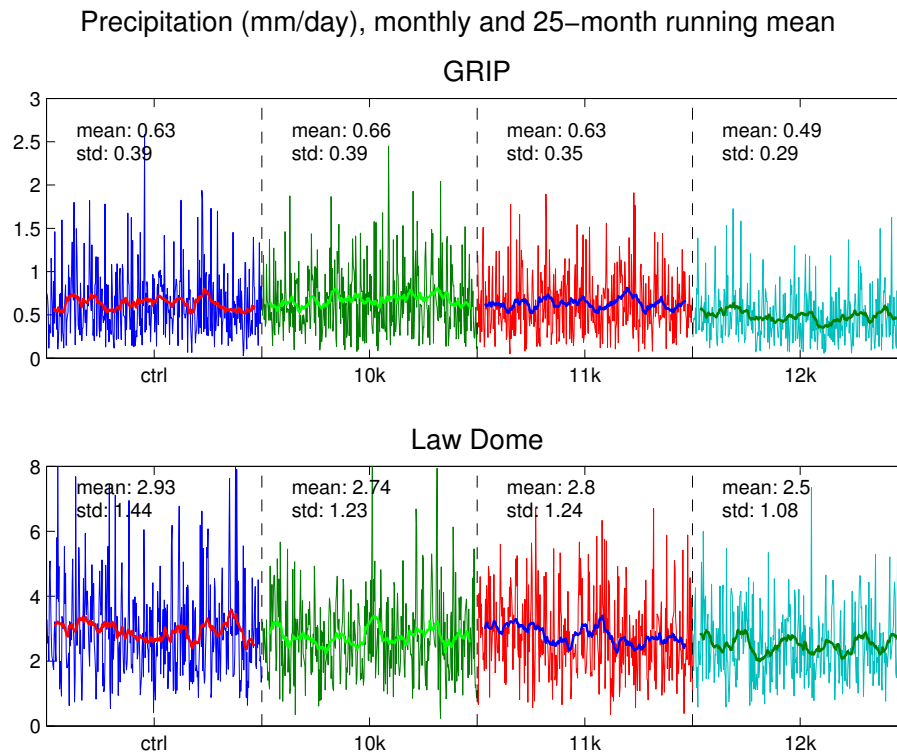
Fig. 5. Precipitation rate ($mm\,day^{-1}$) shown at the GRIP and Law Dome stations, monthly means and 25 month running means.
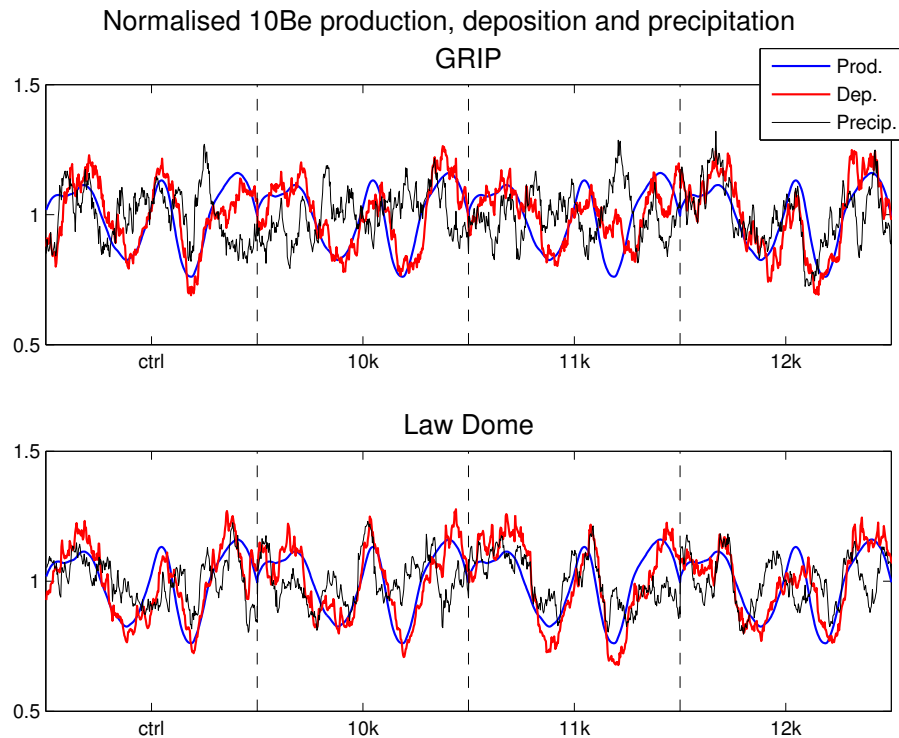
Fig. 6. The input data for the EEMD analysis: normalised 25 month running mean [^10]Be production (blue), deposition (red) and precipitation (black) at the GRIP and the Law Dome stations.

Title Page

Abstract · Introduction

Conclusions · References

Tables · Figures

|◄ · ►|

◄ · ►

Back · Close

Full Screen / Esc

Printer-friendly Version

Interactive Discussion

Full Screen / Esc

Printer-friendly Version

Interactive Discussion
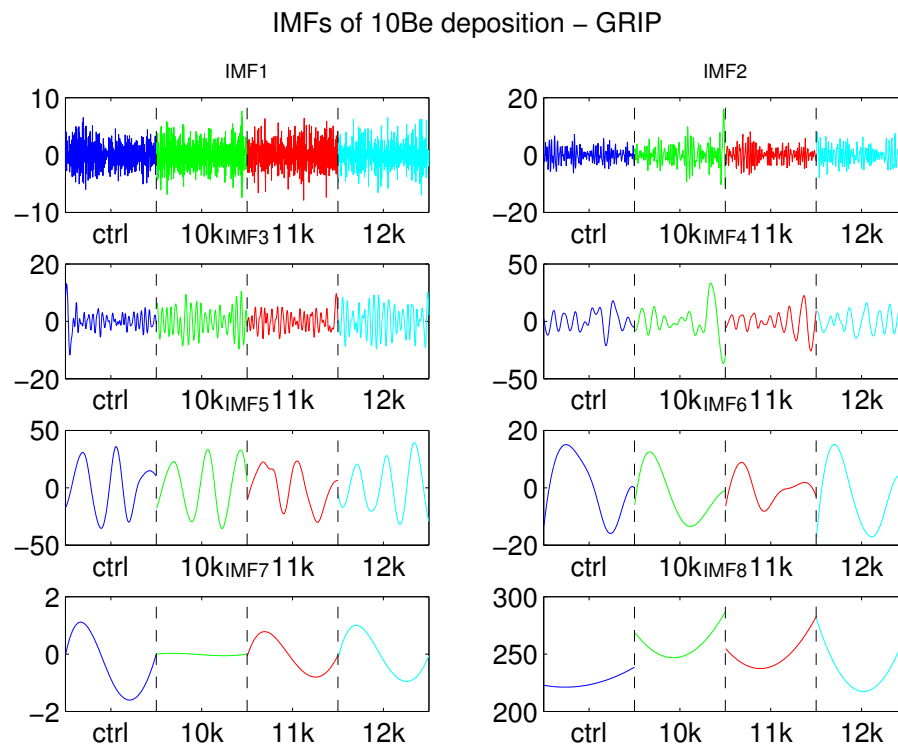
Fig. 7. The seven intrinsic mode functions (IMF1–7) and the long-term trend (IMF8) of [10]Be deposition (atoms $m^{-2} s^{-1}$) at the GRIP station.
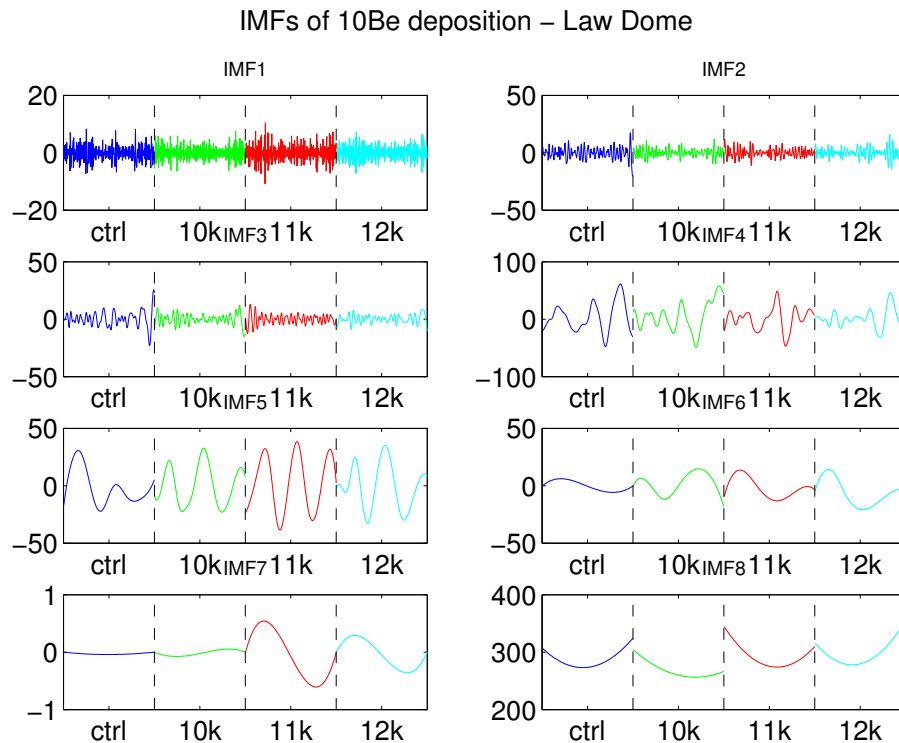
Fig. 8. The seven intrinsic mode functions (IMF1–7) and the long-term trend (IMF8) of ^{10}Be deposition (atoms m^{-2} s^{-1}) at the Law Dome station.
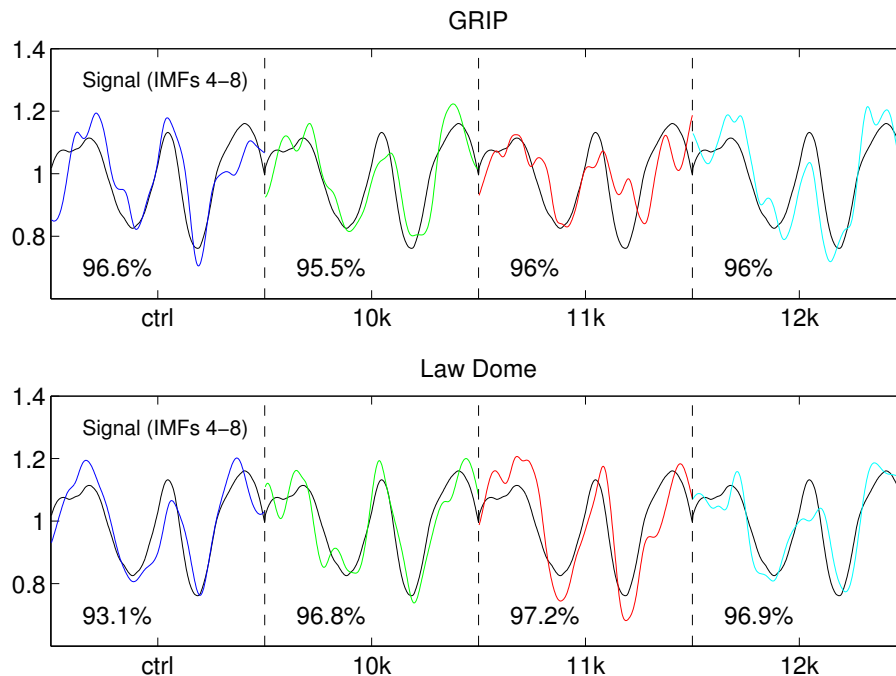
Fig. 9. The normalised reconstructed solar, or ^{10}Be production, "signal" (IMFs 4–8) from the ^{10}Be deposition with the high-frequency noise removed for the four simulations, compared with the normalised original production signal (black). The percentages show the variability explained by the "signal" components in each simulation.
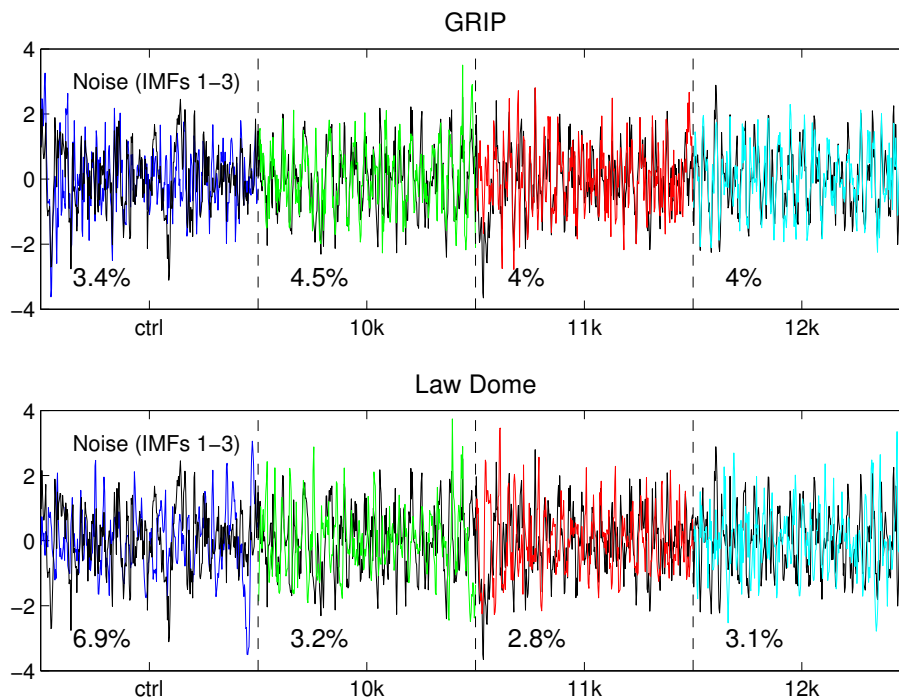
Fig. 10. The standardised reconstructed high-frequency "noise" (IMFs 1–3) from the ¹⁰Be deposition for the four simulations, shown with the same standardised high-frequency components of precipitation (black). The percentages show the variability explained by the "noise" components in each simulation.
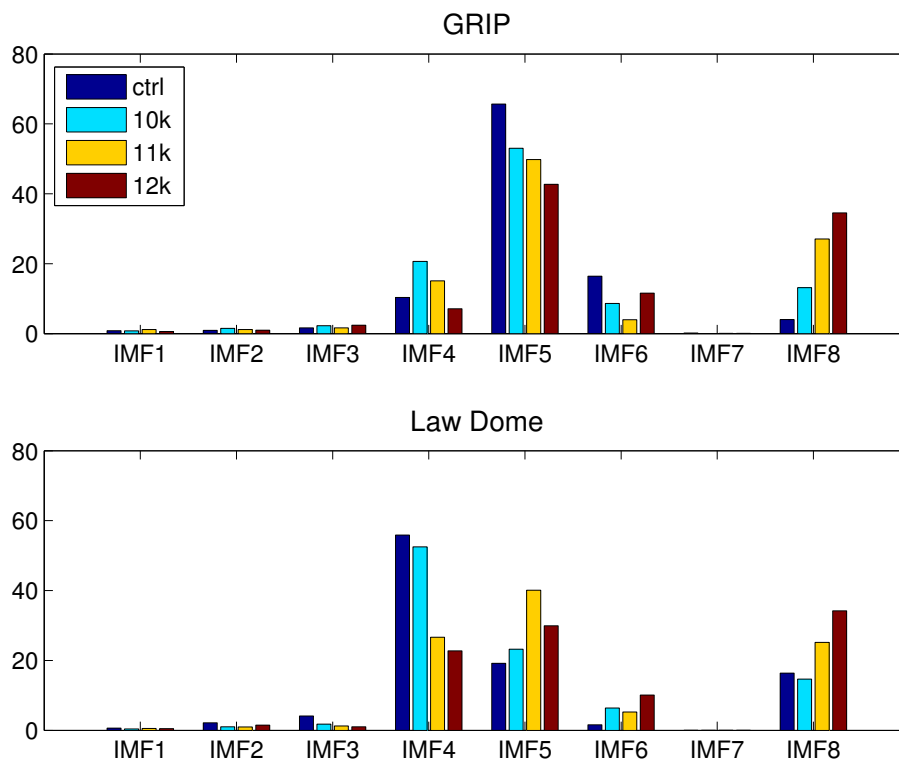
Fig. 11. Variability (%) explained by each IMF of [10]Be deposition for all simulations, both at GRIP (top) and Law Dome (bottom).

10Be in deglaciation – Part 2: Isolating solar signal
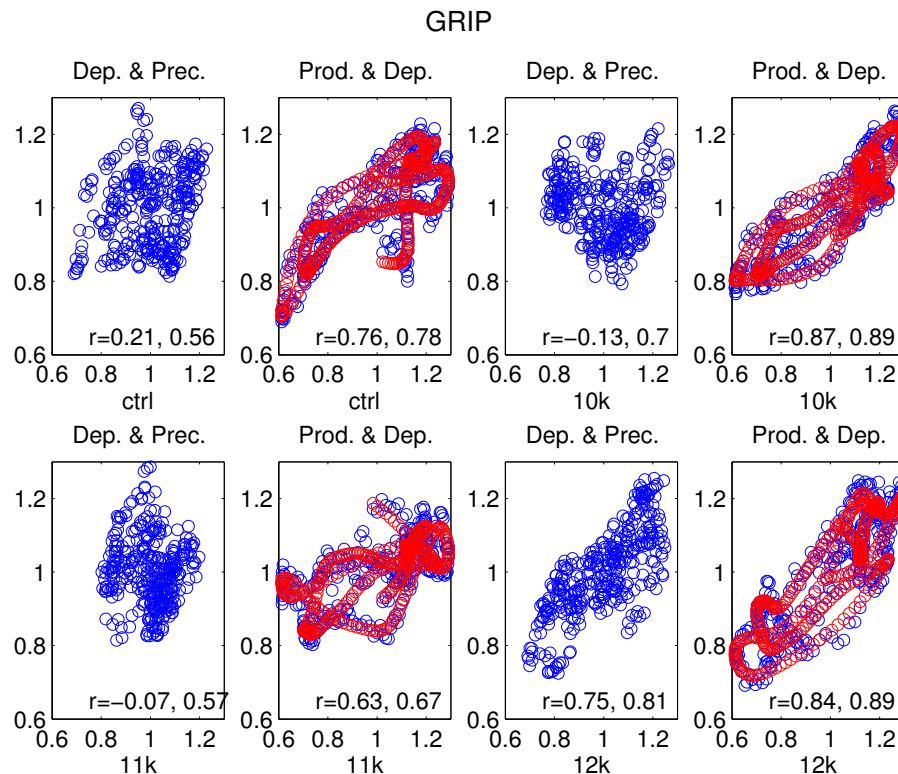
U. Heikkilä et al.

GRIP

Fig. 12. In blue: scatter plots and correlation coefficients (first numbers) between variables (production: "Prod.", deposition: "Dep." and precipitation: "Prec.") of 25 month running means at the GRIP station. In red: scatter plots and correlation coefficients (second numbers) between the noise-filtered (IMFs 4–8) production and deposition.

[10]Be in deglaciation – Part 2: Isolating solar signal
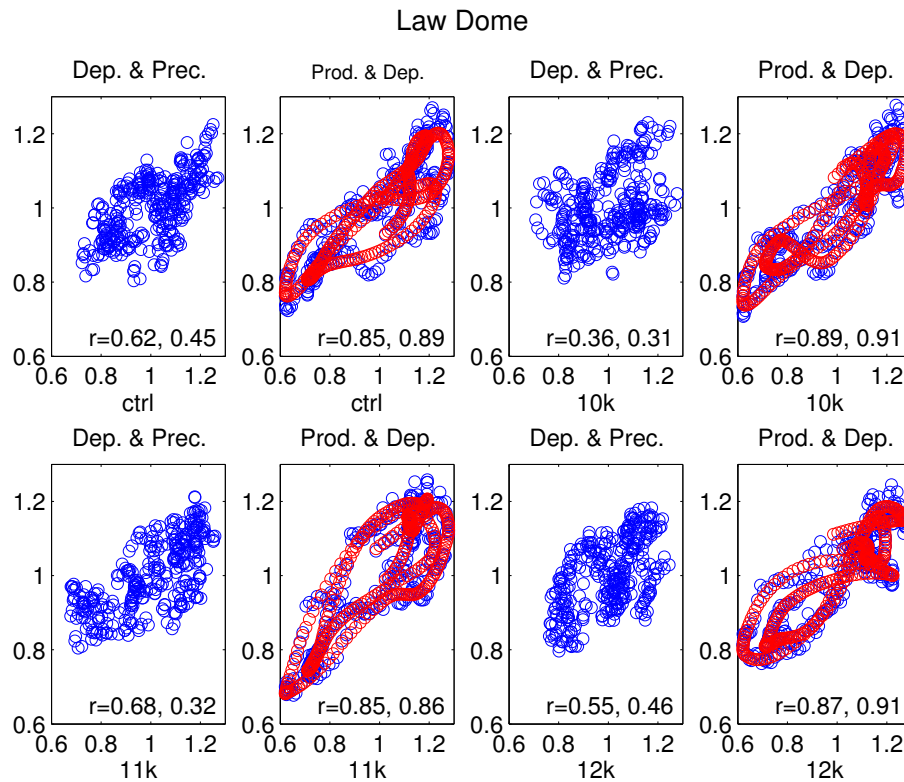
U. Heikkilä et al.

Fig. 13. Same as Fig. 12 but for the Law Dome station.